DOI 10.5012/bkcs.2011.32.4.1204

Lithium Insertion Behavior of Nanoscopic Co_3O_4 Prepared with Avian Egg Membrane as a Template

Maria Christy,[†] Jisha. M. R,[‡] Ae Rhan Kim,[‡] Kee Suk Nahm,[†,‡] Dong Jin Yoo,[‡] E. K. Suh,[†,*] T. Sri Devi Kumari,[§] T. Prem Kumar,[§] and A. Manuel Stephan[§]

[†]*School of Semiconductor and Chemical Engineering, and Semiconductor Physics Research Center, Chonbuk National University, Chonju 561-756, Korea. [*]E-mail: eksuh@chonbuk.ac.kr*
[‡]*Specialized Graduate School of Hydrogen and Fuel Cells Engineering, Chonbuk National University, Chonju 561-756, Korea*
[§]*Electrochemical Power Systems Division, Central Electrochemical Research Institute, Karaikudi 630006, Tamil Nadu, India*
Received November 1, 2010, Accepted February 6, 2011

Nanoscopic Co_3O_4 particles were prepared using avian egg membrane as a template at 800 °C. The prepared materials were subjected to XRD, SEM, TEM and Raman spectroscopic studies. Cyclic voltammetry study shows a single step oxidation and reduction process. Electrochemical lithium insertion behavior of the materials was examined in coin cells of the 2032 configuration. The material showed a discharge capacity 600 mAh/g even after 20 cycles.

Key Words: Oxides, Nanostructures, Electron microscopy, Electrochemical properties

Introduction

The evolution of lithium-ion batteries can be traced to problems associated with the use of metallic lithium in rechargeable lithium batteries. Although graphite is the most popular anode material in lithium-ion batteries, with a specific capacity of only 372 mAh/g, it fares poorly compared to metallic lithium with a specific capacity of 3862 mAh/g. Thus, great efforts are being made towards development of a variety of other anode materials such as lithium-alloying metals, electro-active polymers and silicon. Research in such high-capacity anode materials is driven by demanding power requirements in emerging applications as in electric vehicles. Conventional wisdom on electrochemical insertion reactions in lithium-ion batteries requires electronically conducting electrode materials with crystallographic voids that can support lithium diffusion. In that sense, interstitial-free 3*d*-metal oxide structures are considered unsuitable for intercalation chemistry. Recently, however, there has been a spurt in papers reporting the use of several oxides, oxysalts, nitrides, fluorides, phosphides, sulphides and borides as anode materials for lithium-ion battery chemistry.[1-7] Tarascon *et al*.[1,2] described the associated reactions, which can involve as many as four electrons per 3*d* metal,[2] as conversion reactions. The active material is created internally by an initial conversion reaction in which the compounds react with lithium to yield nanometallic particles.[1,2,8,9] Reversible capacities as high as 1000 mAh/g have been realized with such conversion anodes. It is also possible to realize an improvement in cyclability if mesoporous structures can be generated by reaction with lithium through insertion or conversion processes.[10-13] For example, β-MnO_2 in its bulk state is electrochemically inactive while in mesoporous form it can react reversibly react with 0.92 lithium.[11,13]

Several groups have investigated the spinel structured Co_3O_4 as an anode material in lithium-ion batteries.[1,14-16] Various synthetic routes have been adopted for the synthesis of this material: thermal deposition (300-400 °C),[11] chemical spray pyrolysis (350-450 °C),[12] chemical vapor deposition (550 °C),[13] pulsed laser deposition,[14] traditional sol-gel method (above 260 °C)[15] and hydrothermal synthesis (180 °C),[16] etc. He *et al*.[17] synthesized Co_3O_4 nanoparticles through oriented aggregation. In a different approach Patrissi and coworkers[18] adopted a template-assisted sol-gel method for the synthesis of Co_3O_4. One-dimensional Co_3O_4 tube structures have also been reported by Shi *et al*.[19] Very recently, the advantages of using egg shell membranes for the synthesis of hierarchically ordered macroporous particles with high surface area was introduced by Yang and coworkers.[20] The method is simple and inexpensive. In this paper, we describe the lithium insertion behavior of conversion electrodes based on Co_3O_4 prepared with avian egg shell membrane as a template.

Experimental

Sample Preparation. The procedure for the preparation of Co_3O_4 is similar to the one adopted by the authors for the synthesis of $LiMn_2O_4$ described elsewhere.[21] Fresh eggs obtained from a local poultry were carefully broken at the blunt end and were emptied of their contents. The eggshells were repeatedly washed in water, and the inner shell membrane and the limiting membrane were removed with a pair of tweezers. The eggshells with the outer shell membrane were dipped in 2 M HCl to dissolve the calcium carbonate shell. The undissolved outer membrane was washed thoroughly with water and dried in an air oven maintained at 40 °C. The dried membranes were then soaked in a methanol solution of $Co(NO_3)_2{\cdot}6H_2O$, the excess solution swabbed with a filter

paper, and dried at 110 °C. The precursor-laden eggshell membranes were subsequently subjected to heat treatment at 800 °C for 10 h.

Characterization. Structural features of the Co_3O_4 product was analyzed by powder X-ray diffraction, microscopic studies and Raman spectrometry. X-ray diffraction patterns were recorded between 10 and 80° on a Rigaku D/Max 2500 X-ray diffractometer fitted with a nickel-filtered Cu K_α radiation source. Raman spectra were recorded on a System-1000 Raman spectrometer with Renishaw software. Particle size and surface morphology of the product were examined by an FE-SEM S-4700 model Hitachi scanning electron microscope and a JEM-2010 model Jeol transmission electron microscope.

Electrochemical Studies. The Co_3O_4 electrodes for electrochemical studies were prepared as follows. A pellet containing 20 mg of the active material and 12 mg of "Teflonized" acetylene black in *iso*-propyl alcohol was pressed and pasted on a nickel mesh current collector (2.0 cm^2), and dried at 100 °C for 12 h in a vacuum oven. The composite Co_3O_4 electrodes were coupled with lithium (Cyprus Foote Minerals) in coin cells of the 2032 configuration. A 1 M solution of $LiPF_6$ in a 1:1 (v/v) mixture of EC-DMC was used as the electrolyte. The cells were assembled in an argon-filled glove box (OMNI-LAB system) in which the oxygen and moisture contents were maintained below 2 ppm. Galvanostatic charge-discharge profiles were recorded between 3.000 and 0.002 V at C/10 rate on a computer-controlled battery-testing unit (BTS 2004, Japan). Slow scan cyclic voltammetric experiments were performed in a three-electrode glass cell in which lithium metal foils served as counter and reference electrodes. The electrolyte used was the same as that for the coin cell. Cyclic voltammograms were run on a Solartron 1287 electrochemical interface at a scan rate of 1 mV/s between 0.005 and 3.000 V.

Results and Discussion

XRD Analysis. The powder X-ray diffraction pattern of the Co_3O_4 synthesized is presented in Figure 1. The high intensities of the peaks suggest a high order of crystallinity of the product. All diffraction peaks are indexable to the pure cubic phase of Co_3O_4 [space group *Fd*3*m* (227)], and are in good agreement with the standard values (JCPDS-ICCD Card No: 42-1467). The absence of any extraneous peaks suggests that the product is single phase and is of high purity. The value of the lattice parameter *a* calculated from the XRD data is 8.101 Å. The value is consistent with those reported for Co_3O_4.[20] The crystallite size of the particles, as calculated by using the Debye-Scherrer relation,[21,22] which relates the full width at half maximum, FWHM, β, of an X-ray peak to its corresponding cosθ value by

$$\beta = \lambda / (\tau \cos\theta) \quad (1)$$

where λ is the incident X-ray wavelength and τ is crystallite size, is 30 nm.

Microscopic Studies. The SEM image of a dried egg membrane template presented in Figure 2(a) shows a macroporous network of interwoven and coalescing membrane fibers with diameters ranging from 0.5 to 2 μm.[21] Furthermore, the voids formed by the interwoven fibers range between 5 and 20 μm. The outer shell membrane of avian eggshells used in this study contains functional groups such as amines, amides and carboxylates,[23] which can help anchor cations. Because of the anchoring, the outer shell membrane should function as a fugitive templating phase. That is, once the membrane with the precursor cations pinned to it gets burnt in the heating step, it leaves behind an ordered macrostructure of the ceramic product, whose morphology

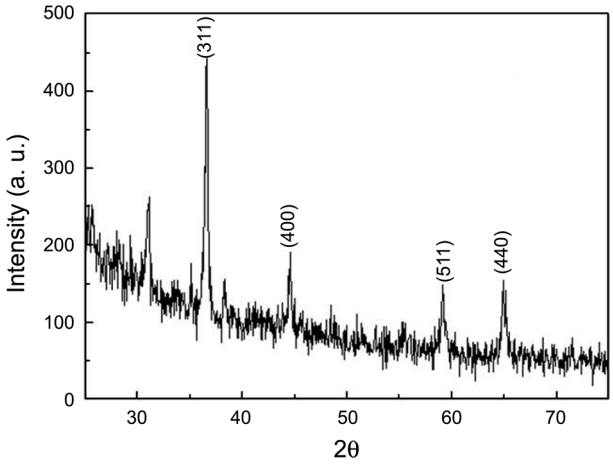

Figure 1. X ray diffraction pattern of Co_3O_4.

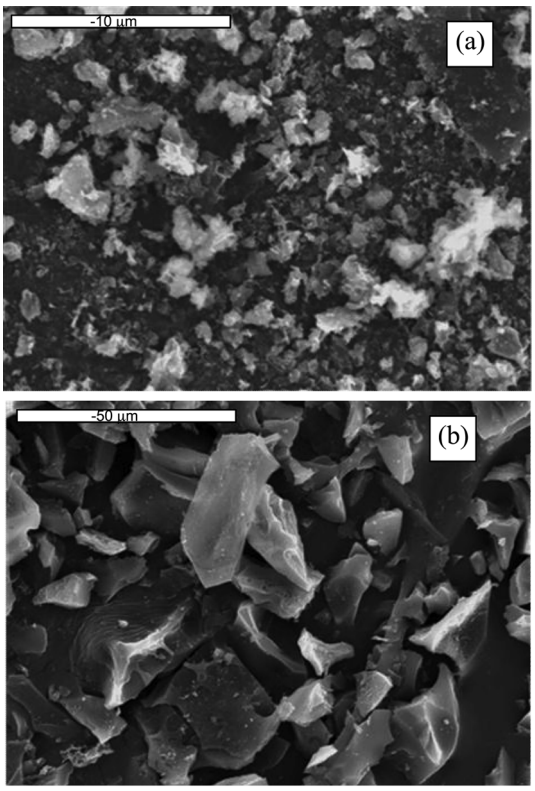

Figure 2. (a) SEM image of dried egg membrane template (b) SEM micrographs of Co_3O_4.

would simply be a replica of the framework structure of the membrane. Figure 2(b) is an SEM image of the Co_3O_4 product, which shows somewhat disjointed flake-like crystals averaging about 600 nm in size distributed in a macroporous matrix with open voids in the range 0.5-2 μm. The smaller open voids in the product suggest that there is a considerable shrinkage in the network structure of the eggshell membrane (from 5-20 μm to 0.5-2 μm) due to loss of moisture and other volatiles from the membrane during the thermal processing.

More insight on the morphology and microstructure was obtained from transmission electron microscopic and high resolution transmission electron microscopic examinations (Fig. 3). The TEM image (Fig. 3(a)) shows rounded, sometimes dumb-bell shaped, particles of size less than 30 nm. In Figure 3(b) are given HRTEM images of individual nanoparticles, which reveal continuous lattice fringes, and thus their high crystalline structure. The observed layer separation corresponds to the (111) planes of Co_3O_4.[20]

Raman Spectroscopy. We carried out Raman spectroscopic analysis of Co_3O_4 in order to confirm its chemical composition and to examine the coordination of the cobalt ions. Normally, Co_3O_4 is crystalline in nature with Co^{2+} and Co^{3+} ions occupying, respectively, the 16*d* octahedral and the *8a* tetrahedral sites in a cubic close packed array of O^{2-} ions, which occupy the 32*e* sites.[24] According to Shebanova and Lazor[25] the A_{1g}, E_g and the three T_{2g} modes are Raman active. Another oxide of cobalt, CoO, possesses a crystalline structure of the face-centered cubic (fcc) type at ambient temperature, in which Co^{2+} ions are octahedrally coordinated

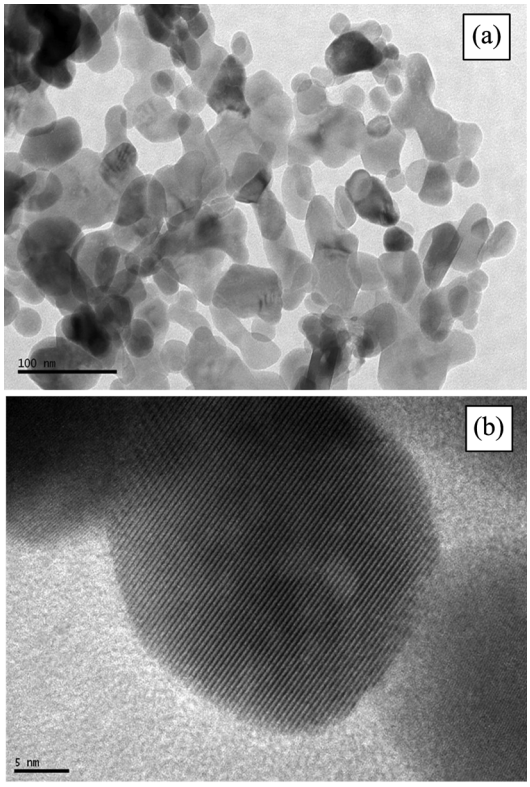

Figure 3. (a) TEM and (b) HR-TEM images of Co_3O_4.

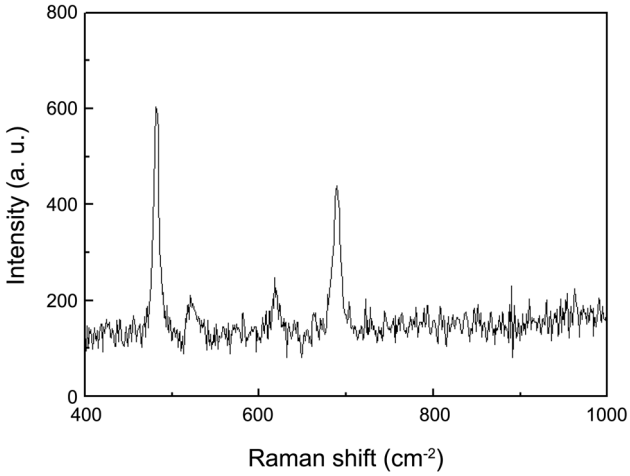

Figure 4. Raman spectrum of Co_3O_4.

to six O^{2-} ions. Theoretically, the O_h symmetry of CoO should also lead to at least three Raman active modes (A_{1g}, E_g and T_{2g}).[14] The Raman spectrum presented in Figure 4 exhibits four well-defined peaks at 484, 514, 609 and 693 cm^{-1}, which can be assigned to the Raman active modes of Co_3O_4, i.e., T_{2g}, E_g, and A_{1g} symmetries, respectively.[26] However, two weak peaks around 510 and 610 cm^{-1} and two intense Raman bands at 470 and 670 cm^{-1} were not noticed in the spectra at ambient conditions. The band at 670 cm^{-1} is attributed to the characteristic of the octahedral sites [CoO_6], which is assigned to the A_{1g} species in the O_h^7 spectroscopic symmetry.[26] The medium intensity Raman bands at 470 and 510 cm^{-1} have the E_g and F_{2g} (2) symmetries, respectively, whereas the weak band at 610 cm^{-1} has the F_{2g} (1) symmetry, which can be depicted as a sum of the (A_{1g}+E_g+2F_{2g}) symmetries.

Electrochemical Studies. The cyclic voltammogram of Co_3O_4 is shown in Figure 5. The first and fifth cycles are indicated separately. A characteristic reduction peak at 1.0 V and a corresponding oxidation peak at 2.18 V can be seen. The reactions associated with the current peaks can be described as follows.

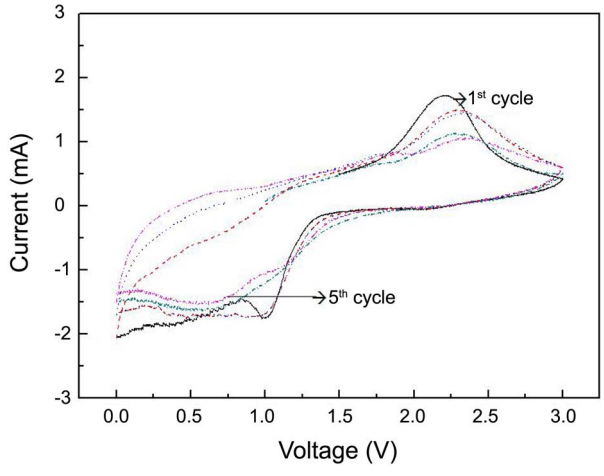

Figure 5. Cyclic voltammogram of Co_3O_4.

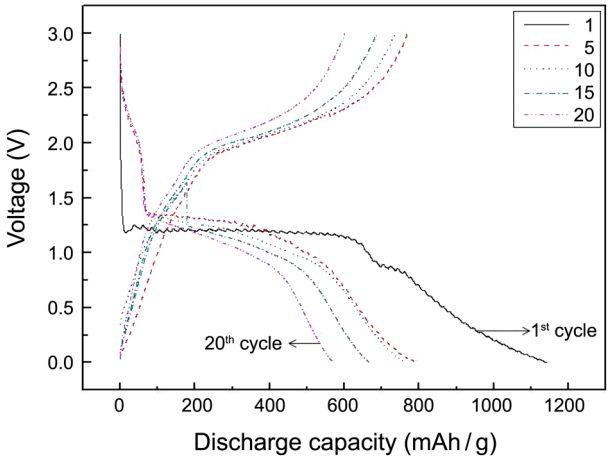

Figure 6. Voltage versus specific capacity of Co_3O_4.

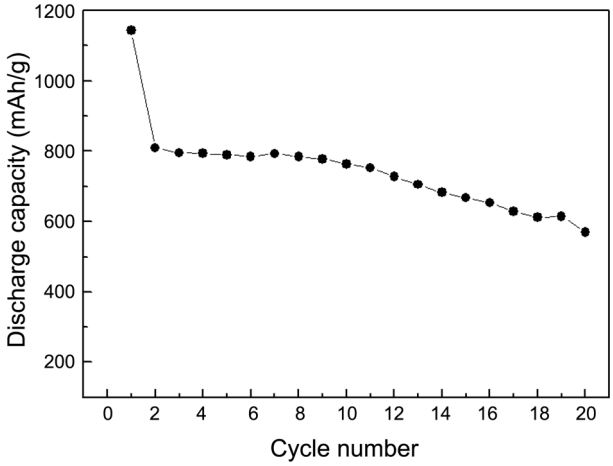

Figure 7. Cyclability of Co_3O_4.

Lithium insertion process:

$$Co_3O_4 + 8\ Li^+ + 8\ e^- \rightarrow 3\ Co + 4\ Li_2O \quad (2)$$

Lithium extraction process:

$$3\ Co + 4\ Li_2O \rightarrow Co_3O_4 + 8\ Li^+ + 8\ e^- \quad (3)$$

It is well established that upon recharge the active material does not revert to the spinel Co_3O_4 oxide but to the monoxide, CoO.[26-28] It can be seen that the difference between the potentials of the peaks get reduced with cycling, suggesting a reduction in polarization from the first cycle (with the as-prepared Co_3O_4) to the subsequent cycles (with the *in situ* formed material).

The charge-discharge profiles of Li/Co_3O_4 cell are displayed in Figure 6. The first-cycle lithium insertion capacity is 1150 mAh/g. However, only 800 mAh/g of lithium could be retrieved, which corresponds to a first-cycle irreversible capacity loss of 30%. This loss in capacity is attributed to the formation of Li_2O in the initial conversion reaction (eq. 2). In the next two cycles the coulombic efficiencies were more than 95%, and reached 100% in the fourth cycle. The profiles are similar to those reported for nano/micro particles of Co_3O_4 reported previously.[16,26-29] There are two distinctively clear potential regions: a flat plateau associated with the conversion reaction and a sloping region ascribed to the formation of a surface layer. In the first cycle, the discharge curve has a plateau at around 1.25 V, which accounts for about 150 mAh/g of the capacity (or a lithium content of 1.5 per Co_3O_4 molecule). According to Tarascon *et al.*,[27] this plateau is due to the formation of α-CoO phase. This is followed by a long plateau, which is associated with Eq. (2).[26,29] Thereafter, the voltage drops falls gradually to the cut-off potential. The sloping voltage region is attributed to the formation of a polymeric surface layer on the electrode particles[30] or to storage of charge/mass at the interface between the Li_2O and Co nanoparticles in the electrode matrix.[31] Bruce *et al.*,[16] based on their results that showed that the capacities represented by the sloping region did not correspond to surface areas of the electrode material, suggest that the dominant charge storage mechanism is formation of a polymeric surface layer.

The discharge capacity (deinsertion capacity) as a function of cycle number is depicted in Figure 7. It can be noted that the material cycles well over the 20 cycles studied thus far. The fade in capacity observed with the present sample (10.75 mAh/g) is much lower than that for Co_3O_4 nanorods prepared by Yang *et al.*[20] The small sizes of the particles in the conversion electrodes together with the polymeric electrolyte layer supposed to be generated in the first lithiation step help buffer strains during the electrochemical process. It must be pointed out that the high surface areas presented by the particles facilitate extensive formation of the polymeric surface layer. The small sizes of the particles in the conversion electrodes together with the polymeric electrolyte layer supposed to be generated in the first lithiation step help buffer strains during the electrochemical process.

Conclusions

We have synthesized macroporous Co_3O_4 made up of crystals averaging 30 nm in size by a replica method using avian eggshell membrane as a template. Like other forms of Co_3O_4-based conversion electrodes, this product also undergoes conversion reaction evidenced by a flat potential plateau and a surface polymer film formation reaction in a subsequent sloping potential plateau. Based on the charge input, it can be assumed that during the initial stages of the lithiation reaction, a product of the formula $Li_{1.5}Co_3O_4$ is formed. At C/10 rate, the material delivered capacities around 800 mAh/g. This study demonstrates the use of avian egg membrane as an inexpensive and easily available biological membrane for the preparation of conversion electrodes based on Co_3O_4.

Acknowledgments. This work was supported by Priority Research Centers Program through National Research Foundation (NRF) funded by the Ministry of Education, Science and Technology (2010-0029706). This work was supported by New & Renewable Energy R & D program (2009T100100606) under the Ministry of Knowledge

Economy, Republic of Korea.

References

1. Poizot, P.; Laruelli, S.; Grugeon, S.; Dupont, L.; Tarascon, J. M. *Nature* **2000**, *407*, 496.
2. Tarascon, J. M.; Grugeon, S.; Morcrette, M.; Laruelle, S.; Rozier, P.; Poizot, P. *C. R. Chimie*. **2005**, *8*, 9.
3. Pereira, N.; Dupont, L.; Tarascon, J. M.; Klein, L. C.; Amatucci, G. G. *J. Electrochem. Soc*. **2003**, *150*, A1273.
4. Xue, M. Z.; Fu, Z. W. *Electrochem. Commun*. **2006**, *8*, 1855.
5. Bervas, M.; Mansour, A. N.; Yoon, W. S.; Al-Sharab, J. F.; Badway, F.; Cosandey, F.; Klein, L. C.; Amatucci, G. G. *J. Electrochem. Soc*. **2006**, *153*, A799.
6. Aragón, M. J.; Pérez-Vicente, C.; Tirado, J. L. *Electrochem. Commun*. **2007**, *9*, 1744.
7. Lavela, P.; Ortiz, G. F.; Tirado, J. L.; Zhecheva, E.; Stoyanova, R.; Ivanova, Sv. *J. Phys. Chem*. **2007**, *C111*, 14238.
8. Li, X. D.; Yang, W. S.; Li, F.; Evans, D. G.; Duan, X. J. *J. Phys. Chem. Solids* **2006**, *67*, 1286.
9. Debart, A.; Dupont, L.; Poizot, P.; Leriche, J. B.; Tarascon, J. M. *J. Electrochem. Soc*. **2001**, *148*, A1266.
10. Jiao, F.; Shaju, K. M.; Bruce, P. G. *Angew. Chem. Int. Ed*. **2005**, *44*, 6050.
11. Luo, J. Y.; Zhang, J. J.; Xia, Y. Y. *Chem. Mater*. **2006**, *18*(23), 5618.
12. Jiao, F.; Harrison, A.; Jumas, J. C.; Chadwick, A. V.; Kockelmann, W.; Bruce, P. G. *J. Am. Chem. Soc*. **2006**, *128*, 5468.
13. Jiao, F.; Bruce, P. G. *Adv. Mater*. **2007**, *19*, 657.
14. Thackeray, M. M.; Baker, S. D.; Adendorff, K. T.; Goodenough, J. B. *Solid State Ionics* **1985**, *17*, 175.
15. Larcher, D.; Sudant, G.; Leriche, J. B.; Chabre, Y.; Tarascon, J. M. *J. Electrochem. Soc*. **2002**, *149*, A234.
16. Shaju, K. M.; Jiao, F.; Débart, A.; Bruce, P. G. *Phys. Chem. Chem. Phys*. **2007**, *9*, 1837.
17. He, T.; Chen, D.; Jiao, X. *Chem. Mater*. **2004**, *16*, 737.
18. Patrissi, C. J.; Martin, C. R. *Chem. Mater*. **1997**, *9*, 2544.
19. Shi, X.; Han, S.; Sanedrin, R. J.; Galvez, C.; Ho, D. G.; Hernandez, B.; Zhou, F.; Selke, M. *Nano Lett*. **2002**, *2*, 289.
20. Yang, D.; Qi, L.; Ma, J. *Adv. Mater*. **2002**, *14*, 1543.
21. Sri Devi Kumari, T.; Prem Kumar, T. *Ionics* **2010**, *16*, 61.
22. Cullity, B. D. *Elements of X-ray Diffraction*; Addison-Wesley: New York, 1978; p. 278.
23. Dennis, J. E.; Carrino, D. A.; Yamashita, K.; Caplan, A. I. *Matrix Biol*. **2000**, *19*, 683.
24. Hadjiev, V. G.; Iliev, M. N.; Vergilov, I. V. *J. Phys. C: Solid State Phys*. **1988**, *21*, L199.
25. (a) Shebanova, O. N.; Lazor, P. *J. Solid State Chem*. **2003**, *174*, 474. (b) Shebanova, O. N.; Lazor, P. *J. Chem. Phys*. **2003**, *119*, 6100.
26. Nakamoto, K. *Infrared and Raman Spectra of Inorganic and Coordination Compounds, Part A: Theory and Applications in Inorganic Chemistry*; Wiley: New York, 1997.
27. Larcher, D.; Sudant, G.; Leriche, J. B.; Chabre, Y.; Tarascon, J. M. *J. Electrochem. Soc*. **2002**, *149*, A234.
28. Fu, Z. W.; Wang, Y.; Zhang, Y.; Qin, Q. Z. *Solid State Ionics* **2004**, *170*, 105.
29. Pralong, V.; Leriche, J. B.; Beaudoin, B.; Naudin, E.; Morcrette, M.; Tarascon, J. M. *Solid State Ionics* **2004**, *166*, 295.
30. Yuan, Z.; Huang, F.; Feng, C.; Sun J.; Zhou, Y. *Mater. Chem. Phys*. **2003**, *79*, 1.
31. Laruelle, S.; Grugeon, S.; Poizot, P.; Dolle, M.; Dupont, L.; Tarascon, J. M. *J. Electrochem. Soc.* **2002**, *149*, A627.
32. Maier, J. *Nat. Mater.* **2005**, *4*, 805.